Listening to Raindrops from Underwater: An Acoustic Disdrometer

JEFFREY A. NYSTUEN

Applied Physics Laboratory, University of Washington, Seattle, Washington

(Manuscript received 24 July 2000, in final form 27 March 2001)

ABSTRACT

Different sized raindrops splashing on a water surface produce sound underwater that is distinctive and can be used to measure the drop size distribution in the rain. Five acoustically significant raindrop sizes are described. An inversion of the underwater sound to measure the drop size distribution in the rain is described and demonstrated. Limitations to the inversion include problems associated with the relative loudness of the largest drops (diameter over 3.5 mm), the relative quietness of the medium drops (diameter 1.2–2.0 mm), and the influence of wind to suppress the signal from the otherwise remarkably loud small drops (diameter 0.8–1.2 mm). Various measures of rainfall, including rainfall rate, equivalent radar reflectivity, median drop size, and other integrated moments of the drop size distribution are measured acoustically and used to examine rainfall research issues. The relationship between equivalent reflectivity and rainfall rate, the *Z–R* diagram, is partitioned acoustically showing that parts of this diagram are occupied by rainfall containing specific drop populations. Rainfall type can be classified acoustically. And because of its relatively large catchment area, high temporal resolution analysis of rainfall is possible. This technique has inherent application in remote oceanic regions where measurements of rainfall are needed to help establish knowledge of the global distribution and intensity of rainfall.

1. Introduction

Rain is one of the most important components of climate, and one of the most difficult to measure. This is because of its inherent inhomogeneity in both time and space. Furthermore, instrumentation to measure rain, especially in oceanic regions, is limited. Data are needed to identify occurrence of rain, type of rainfall, and to quantify rainfall amounts.

Rain is also one of the principal natural sources of underwater sound. The idea that underwater sound can be used as a signal to detect and quantify rainfall at sea (Shaw et al. 1978) has been developed through laboratory studies on individual drop splashes (Pumphrey et al. 1989; Medwin et al. 1990; Medwin et al. 1992; Nystuen and Medwin, 1995) and field studies (Nystuen 1986; Nystuen et al. 1993; Nystuen and Selsor 1997). Because different raindrop sizes produce distinctive sound underwater, the sound field can be decomposed to measure the drop size distribution in the rain (Nystuen 1996). This study extends the Nystuen (1996) result to refine the inversion algorithm, demonstrate its success, and to identify limitations associated with actual measured drop size distributions using an extensive dataset collected in Miami, Florida (Nystuen et al. 1996).

As with any tool to measure rain, one would like to use it to learn about rain. The Miami data are used to examine three rainfall research issues. The relationship between equivalent reflectivity and rainfall rate, the *Z–R* diagram, can be partitioned acoustically and shows that parts of this diagram are occupied by rain containing specific raindrop populations. Rainfall classification has been attempted acoustically (Black et al. 1997). By using the sound field as a disdrometer, additional descriptors of rain are available to extend this classification potential. Finally, the relatively large spatial coverage (catchment area) associated with the underwater sound field allows high temporal analysis of the rain.

2. Experimental data

The data for this study are from a 17-month field experiment in Miami, Florida (Nystuen et al. 1996). An ITC-4123 hydrophone was mounted 1.5 m below the surface in a mangrove-lined pond approximately 30 m from the nearest edge. The mangrove trees averaged 5–7 m in height producing a ''sheltered'' situation with relatively low wind speeds. The signal was cabled to shore and recorded on a 50-MHz 486 PC computer equipped with a Microstar Laboratories DAP 2400/6 12-bit A/D board. Each second a 4096 point time series was recorded at 100 kHz (40.96 ms). A three-stage amplifier was used to increase the dynamic range. Spectral analysis (filter, FFT, and averaging) were applied to reduce the output to a single 128-point acoustic spectrum

Corresponding author address: Dr. Jeffrey A. Nystuen, Applied Physics Laboratory, University of Washington, 1013 NE 40th Street, Seattle, WA 98105-6698.
E-mail: nystuen@apl.washington.edu

(0–50 kHz, 390-Hz resolution, 43 degrees of freedom). This sound spectrum was recorded every second.

Various rain gauges were deployed nearby, including a Joss–Waldvogel (JW) disdrometer, an Scientific Technology Inc. (ScTI) optical rain gauge (ORG), an R. M. Young capacitance rain gauge (CAP), a Belfort 382 tipping-bucket rain gauge, and a custom-built weighing rain gauge. The relative performance of these automatic rain gauges is reported in Nystuen (1999). Of greatest interest in this study are the data from the disdrometer. This instrument measures the drop size of individual drops as they strike the sensor head. The sensor head has a surface area of 50 cm^2. Drops are counted into 20 drop size bins, ranging from 0.3-mm to over 5-mm diameter. The data were accumulated for 1 min, and recorded each minute. For comparison purposes, the temporal resolution of the other rain gauges, including the acoustical data, were averaged to 1-min temporal resolution.

Although over 9100 min of rainfall were recorded during the experiment, this study will concentrate on over 6000 min of rainfall data collected from April to December 1994. These data include rainfall from subtropical convective systems, including small local events, larger mesoscale convective systems (MCS) and one tropical cyclone [Tropical Storm (TS) Gordon in Nov 1994]. Within events, different types of rainfall include initial convection, heavy and extremely heavy convection, transition, and stratiform types I and II, as described by Atlas et al. (1999).

Several examples of the sound spectrum recorded during rainfall, with the associated drop size distribution from the disdrometer, are presented in Fig. 1. These are representative of the different ''types'' of rainfall that were observed during the experiment and illustrate some of the important features of the underwater sound that are closely associated with the rainfall drop size distribution within the rain. These features are consistent with laboratory studies of sound generated by individual raindrops (Medwin et al. 1992; Nystuen and Medwin 1995). When the rain contains small raindrops (0.8–1.2-mm diameter), a strong acoustic signal is present from 13 to 25 kHz. This feature is most apparent when the rain does not have larger raindrops present. When the rain contains large raindrops (2.0–3.5-mm diameter), the sound level below 10 kHz is loud and there is often a relative peak in the sound spectrum at a frequency between 2 and 5 kHz. If very large raindrops (greater than 3.5-mm diameter) are present, the signal is very loud and extends from 1 to 50 kHz. However, during extreme rainfall rates (over 100 mm h^{-1}) the shape of the sound spectrum often changes and becomes relatively steep above 30 kHz. This feature of the sound spectrum is likely to be associated with subsurface bubbles and will be discussed in more detail later. In all cases, the signal from the rain is very loud, sometimes as much as 50 dB above the background noise level.

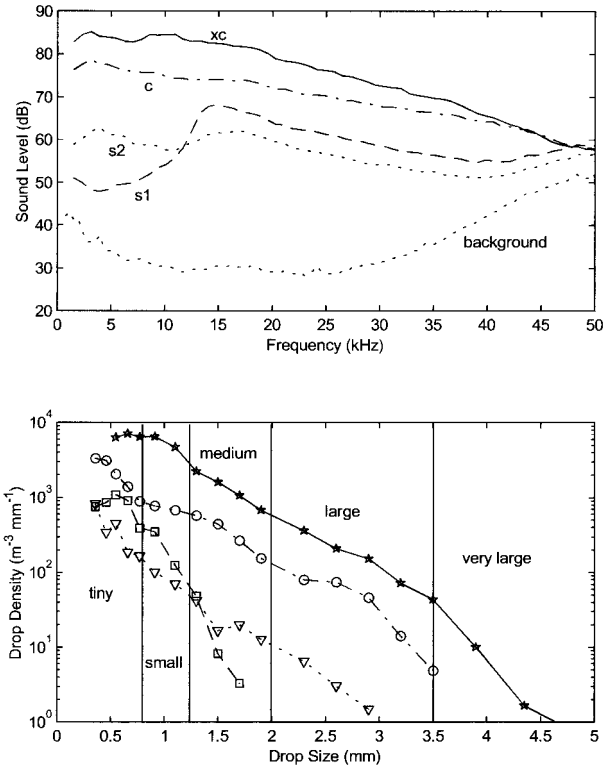

FIG. 1. Examples of observed sound fields and the associated drop size distributions within the rain. (top) The examples are labeled by rainfall type: xc (extreme convection, solid line, ★, ID = 150_47); c (moderate convection, dash–dot, ○, ID = 114_39); s2 (stratiform II type rain, dotted line, ▽, ID = 54_11), and s1 (stratiform I, dashed line, □, ID = 150_30). Various values of rainfall parameters are given in Table 1 for each of these examples. (bottom) Different acoustic raindrop sizes.

3. Background

a. Describing rainfall

The ultimate description of rainfall is the actual drop size distribution within rain. This is quite variable in time and space. It changes for different types of rainfall. This is of significance meteorologically as different types of rainfall have different heating profiles within the atmosphere and thus affect atmospheric dynamics in different ways (Houze 1989). Within the MCSs prevalent within these data, two general types of rainfall are recognized: convective and stratiform. Identifying these rainfall types is also important for rainfall measurement instruments, as most measurements are integral moments of the drop size distribution and different types of rainfall have different relative drop size distributions. For example, a radar measures reflectivity, Z, the 6th moment of the drop size distribution. If the measurement of interest is rainfall rate R, approximately the 3.6th moment of the drop size distribution, then an inherent ambiguity is present (Ulbrich and Atlas 1978). By first identifying rainfall type, different Z–R relationships can be used which should improve the rainfall rate mea-

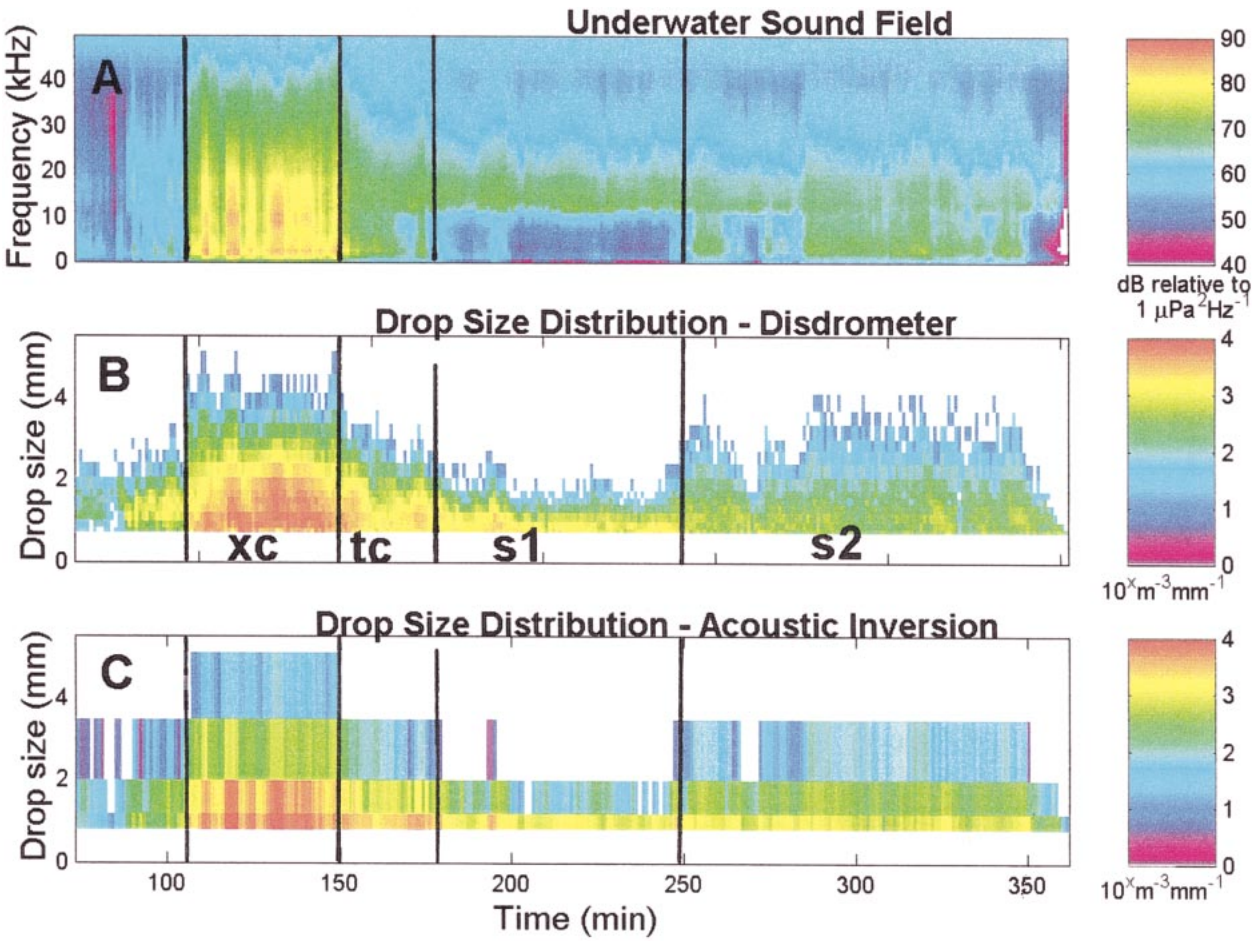

FIG. 2. (a) The sound field, (b) observed drop size distribution, (c) and acoustical inversion of the sound field to obtain drop size distribution for event 150 at 0113 LT (event 150 at 0113). [Note: the event ID is given by the Julian day in 1994 followed by the start time. Event 150 at 0113 occurred on day 150, 30 May, starting at 0113 local time.] The units for the sound field are in decibels relative to 1 μPa^2 Hz^{-1}. The units for drop size distribution are 10^x m^{-3} mm^{-1}, where x is shown by the color bar. The different rainfall types, following the study of Atlas et al. (1999), are extreme convection (xc), transition/convection (tc), stratiform I (s1), and stratiform II (s2), and are indicated by the vertical lines.

surement from radars (Steiner et al. 1995; Tokay and Short 1996). The spatial and temporal scales of stratiform rain are much larger than convective rain, allowing classification by spatial analysis (Rosenfeld et al. 1995a,b).

Recently, Atlas et al. (1999) have extended the classification of rainfall types by noting systematic variations of the surface drop size distributions within the convective and stratiform classifications of rainfall. These extended classifications of rainfall are apparent within the Miami rainfall dataset. An example of a MSC system, showing the observed sound field and the drop size distributions is shown in Fig. 2. Two convective and two stratiform categories are identified from the disdrometer data following the analysis of Atlas et al. (1999). The convective portions of the rain in Fig. 2 consisted of an extreme convective cell (xc) in which the rainfall rates exceeded 100 mm h^{-1} (extreme rain), and a transitional period following the main cell (tc) in which both convective and stratiform rainfall are thought to coexist (Williams et al. 1995). The stratiform portions of the MSC are labeled s1 and s2. The stratiform I rain consists of mostly small raindrops, while the stratiform II rain contains large drops and relatively fewer small drops. In the Atlas et al. (1999) study, a strong brightband (melting of hydrometeors at the freezing level) was associated with stratiform II rainfall.

Examination of the associated sound field (Fig. 2a) shows that these four categories of rainfall have distinctive acoustical signatures, strongly suggesting that analysis of the sound field can help to identify rainfall type. The character of the sound spectra shown in Fig. 2 is consistent with the examples shown in Fig. 1. When the rain contains very large raindrops (over 3.5-mm diameter), the sound is loud from 1 to 50 kHz. If the rain contains large drops (over 2.0-mm diameter), the sound levels below 10 kHz are elevated. If the rain contains small drops (0.8–1.2-mm diameter), there is a

strong acoustic signal from 13 to 25 kHz. (Also shown as in Fig. 2c is the acoustic inversion of the sound field to obtain drop size distribution. This is a principal result of this paper and will be described in more detail later.)

Quantification of the classifications shown in Fig. 2 requires identification of measurable features of the drop size distribution of the rain. These can be integrated quantities such as rainfall rate or equivalent reflectivity, or they can be parameters of the drop size distribution. The exact drop size distribution is often complicated, and so analytic approximations are often used. Two forms are most often used: an exponential distribution (Marshall and Palmer 1948):

$$N(D) = N_0 e^{-\Lambda D}, \tag{1}$$

where N_0 varies and Λ is a function of rainfall rate, and a gamma distribution (Ulbrich 1983):

$$N(D) = N_G D^{\mu} e^{-\Lambda D}, \tag{2}$$

where μ is a shape parameter having both positive or negative values. In this expression, the units of N_G include μ (m^{-3} $mm^{-1-\mu}$) and are difficult to interpret physically. One additional descriptor of rain that is often used is the median drop diameter by volume (Ulbrich 1983). This is given by

$$D_0 = \frac{(3.67 + \mu)}{\Lambda}. \tag{3}$$

Figure 3 shows several of these quantities for the rain event shown in Fig. 2, and Table 1 gives some values of these parameters for specific minutes, including the examples shown in Fig. 1. Note that Figs. 2 and 3 also show the acoustic inversion results for future comparison purposes. As can be seen in Fig. 3, there are systematic variations in the descriptors of rainfall that can be used to identify the different types of rainfall (Atlas et al. 1999). During the extreme convective (xc) rain, the values of R, Z, N_0, and D_0 are all relatively high. In this example, the rainfall rates are over 100 mm h, and Z is greater than 50 dBZ. Atlas et al. (1999) suggest two additional convective rainfall partitions: an initial convective (ic) component when the rain consists of relatively few, but very large raindrops (D_0 is very large, N_0 is very small), and a transition component consisting of a mixed stratiform/convective rainfall components (tc) (Williams et al. 1995) often at the trailing edge of the main convective rain cell during which D_0, Z, and R are all decreasing. Two types of stratiform rainfall are recognized. Stratiform I (s1) consisting of only small raindrops (D_0 is small, N_0 is large), often immediately following the transition period, and stratiform II (s2) consisting of both large and small raindrops (D_0 is large, N_0 is small). Temporally, s1 and s2 rains can persist for many minutes, sometimes hours. (Note that for a specific rain event, the convective and stratiform components may occur in a variety of temporal positions depending on the geometry of the storm and the location of the observations.)

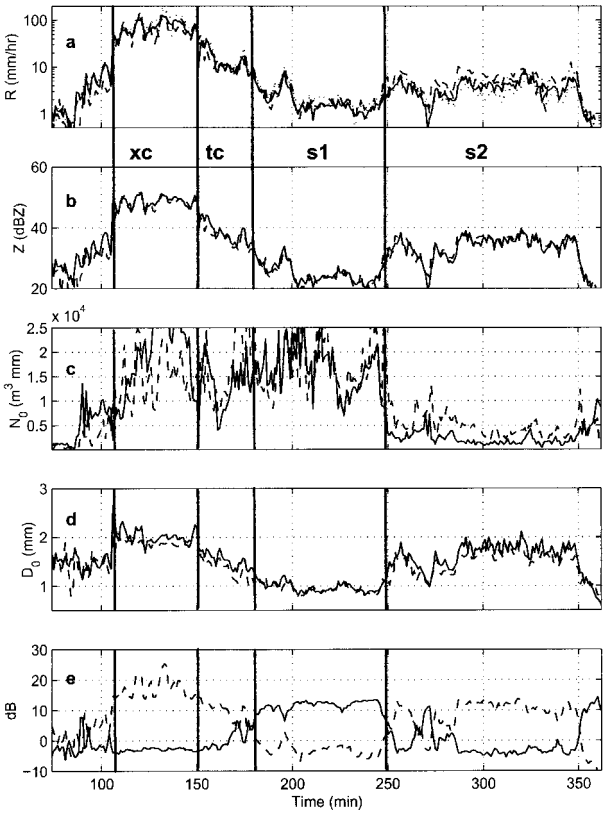

FIG. 3. Various parameters of the rainfall for event 150 at 0113. (a) Rainfall rate measured by the JW disdrometer (solid line), the acoustic inversion (dashed line), the capacitance rain gauge (dotted line), and the optical rain gauge (dash–dot line). (b) The equivalent reflectivity calculated from the JW disdrometer (solid line) and the acoustic inversion (dashed line). (c) N_0 [Eq. (1)] calculated from the JW disdrometer (solid line) and the acoustic inversion (dashed line). (d) D_0 calculated from the JW disdrometer (solid line) and the acoustic inversion (dashed line). (e) Two acoustic discriminants: the modified Black et al. discriminant [Eq. (4); solid line] and the new bubble discriminant [Eq. (5); dashed line].

Two quantifications of the sound field are also plotted in Fig. 3. These are the ratio of sound levels in the 10–30-kHz band compared to the 4–10-kHz band. This quantity was identified by Black et al. (1997) and is referred to as an acoustic discriminant,

$$\mathrm{DR}_{\mathrm{driz}} = \mathrm{SPL}_{10\text{–}30} - \mathrm{SPL}_{4\text{–}10}, \tag{4}$$

where SPL_x is the sound pressure level in decibles relative to 1 μPa^2 Hz^{-1} in the frequency band given by x (in kHz). Black et al. (1997) use this quantity to distinguish between convective and stratiform rainfall. A second potential discriminant is proposed here,

$$\mathrm{DR}_{\mathrm{bubbles}} = \mathrm{SPL}_{4\text{–}10} - \mathrm{SPL}_{40\text{–}50}, \tag{5}$$

and will be used to acoustically identify the presence of subsurface bubbles. These two acoustic descriptors of rainfall will be discussed in more detail later.

TABLE 1. Rainfall measurements for selected data from different rainfall types. The rainfall types are ic (initial convective consisting of a few very large raindrops), xc (extreme convective—over 100 mm h^{-1}), c (convective or transition), s2 (stratiform with large drops and relatively few small drops), and s1 (stratiform with few large drops and relatively more small drops). The ID includes the Julian date of the event and the minute within the event, e.g., 114_18 is min 18 of the event on Day 114 (the highest rainfall rate minute of the entire dataset). Integrated rainfall measurements include rainfall rate (R_d, R_a, R_c, R_o) from the disdrometer, acoustic inversion, capacitance gauge, and optical gauge, respectively. Equivalent reflectivity Z, median drop size D_0, Marshall–Palmer exponent N_0, and gamma distribution shape parameter μ are calculated from the drop size distribution measured by the disdrometer (Z_d, D_d, N_c, μ_d) and the acoustic inversion (Z_a, D_a, N_a, μ_a), respectively. Two sound field parameters, the drizzle discriminant DR_{driz} [Eq. (4)] and the bubble discriminant DR_{bub} [Eq. (5)] are also presented. If the data from a particular minute appears elsewhere in a figure, the figure number is given.

	Rainfall type and ID	Rainfall rates				Reflectivity		D_0		$\log_{10}N_0$		Gamma μ		Discriminants	
		R_d	R_a	R_c	R_o	Z_d	Z_a	D_d	D_a	N_d	N_a	μ_d	μ_a	DR_{driz}	DR^{bub}
	ic 161_6	21.3	31.5	27.7	7.5	47.9	47.5	3.1	2.0	3.0	3.6	7.2	−0.6	−3.7	8.3
Fig. 1:	xc 150_47	147.1	115.3	140.1	142.3	52.2	51.5	1.9	1.9	4.6	4.4	1.4	0.7	−3.4	22.0
Fig. 6a:	xc 114_18	240.4	265.5	368.9	259.1	54.7	55.8	2.2	2.3	4.7	4.6	7.0	3.1	−10.6	27.3
	xc 161_26	118.0	159.0	136.7	137.1	51.4	53.9	2.0	2.2	4.5	4.3	1.9	2.1	−6.8	20.1
Fig. 16:	xc 256_33	104.0	103.5	126.0	125.0	51.8	50.9	2.2	2.0	4.2	4.4	3.0	0.7	−3.3	22.2
	xc 150_60	119.0	112.5	140.9	180.9	45.5	43.6	2.0	1.9	4.5	4.4	7.4	0.0	−3.2	25.5
Fig. 6b:	c 256_39	52.0	42.3	60.9	77.5	46.5	46.1	1.8	1.9	4.3	4.1	2.6	2.1	−2.7	14.8
	c 184_23	23.7	29.5	23.0	22.7	44.0	44.2	1.8	1.8	3.8	4.0	0.8	2.5	−3.1	14.1
Fig. 1:	c 114_39	33.0	30.3	31.2	34.9	45.1	45.2	1.9	2.0	4.0	3.8	2.6	2.5	−4.1	14.9
	c 114_42	17.8	16.9	18.4	21.0	40.7	39.6	1.6	1.5	4.1	4.0	3.4	2.2	−3.2	14.1
Fig. 6c:	c 256_50	12.8	8.0	13.7	13.6	38.4	35.5	1.5	1.3	4.1	4.0	3.4	1.9	−0.4	10.3
	c 184_55	6.5	6.4	7.3	7.9	34.4	34.6	1.2	1.4	4.1	3.9	1.3	1.9	−0.5	10.0
	s2 150_240	4.6	6.6	6.5	3.4	37.1	36.8	1.9	1.7	3.1	3.5	1.3	3.3	−4.1	12.1
	s2 256_123	4.4	5.8	4.5	3.3	35.4	36.3	1.6	1.7	3.4	3.4	1.7	3.6	−4.7	14.8
Fig. 1:	s2 154_11	1.9	1.7	1.6	1.5	31.0	29.5	1.5	1.4	3.2	3.2	1.4	1.9	−1.5	6.2
	s2 184_29	3.1	2.7	3.5	2.2	32.6	31.1	1.5	1.4	3.5	3.5	2.1	1.9	−2.4	10.7
Fig. 1:	s1 150_130	1.3	0.8	1.2	1.1	22.6	19.5	0.9	0.8	4.3	4.2	6.4	9.0	12.9	−5.9
	s1 184_84	2.4	1.5	2.9	3.6	26.2	24.1	1.0	1.0	4.4	4.1	6.9	5.0	11.3	−0.5
	s1 114_72	2.1	2.4	1.5	2.0	25.6	26.5	1.0	1.0	4.3	4.2	13.0	5.1	10.5	1.5
Fig. 6d:	s1 256_68	0.1	0.4	0.4	0.4	10.1	19.9	0.8	1.2	3.8	3.1	9.7	10.2	12.9	−7.4

TABLE 2. Acoustic raindrop sizes. The raindrop sizes are identified by different physical mechanisms associated with the drop splashes (Medwin et al. 1992; Nystuen 1996). These definitions for raindrop sizes will be used throughout this paper.

Drop size	Diameter	Sound source	Frequency range	Splash character
Tiny	<0.8 mm	Silent		Gentle
Small	0.8–1.2 mm	Loud bubble	13–25 kHz	Gentle, with bubble every splash
Medium	1.2–2.0 mm	Weak impact	1–30 kHz	Gentle, no bubbles
Large	2.0–3.5 mm	Impact Loud bubbles	1–35 kHz 2–35 kHz	Turbulent irregular bubble entrainment
Very large	>3.5 mm	Loud impact Loud bubbles	1–50 kHz 1–50 kHz	Turbulent irregular bubble entrainment penetrating jet

b. Underwater sound generated by rain

The underwater sound of the rain is the sum of the sound generated by the individual drop splashes. Different physical mechanisms for sound production by different size raindrops have been identified in laboratory studies (Pumphrey et al. 1989; Medwin et al. 1992; Nystuen and Medwin 1995). Two general mechanisms are present: the trapping of a bubble underwater during the splash and the impact of the drop onto the water surface. Except for the largest drops, the sound radiated by a bubble dominates the sound production and is confined to a very narrow frequency band. The center frequency for acoustic radiation and absorption is associated with the bubble size:

$$f = \frac{1}{2\pi a}\sqrt{\frac{3\gamma P_0}{\rho_0}}, \tag{6}$$

where f is the resonance frequency, a is the bubble diameter, P_0 and ρ_0 are the local pressure and density, and γ is the ratio of specific heats for air ($\gamma = 1.4$). The size of the bubble depends on the physics of the splash, which in turn depends on the raindrop size, shape, angle of impact, and impact speed.

For naturally occurring raindrops in the size range 0.8–1.2-mm diameter, the geometry of the splash results in the regular entrainment (every drop splash) of a bubble that resonates between 13 and 20 kHz (Pumphrey et al. 1989; Oguz and Prosperetti 1990; Longuet-Higgins 1990). This drop size will be referred to as ''small'' raindrops. The sound produced by these small raindrops will be referred to as the ''sound of drizzle,'' as these small raindrops are present in most rain, including very light rain. This sound production mechanism is sensitive to the angle of impact (Medwin et al. 1990), and indeed, the sound of drizzle is observed to be dependent on wind speed (Nystuen 1993). The impact component of sound generated by small raindrops is very small when compared to the sound produced by the bubbles.

Once the raindrop size exceeds 1.2-mm diameter, the geometry of the splash no longer supports regular bubble entrainment. In fact, ''medium'' raindrops, 1.2–2.0-mm diameter, are relatively quiet when compared to small raindrops. Their splashes do not generate underwater bubbles. This feature makes the medium raindrops relatively difficult to hear and quantify.

Larger raindrops have turbulent splashes which allow entrainment of bubbles by at least two different mechanisms (Nystuen and Medwin 1995). These bubbles are produced irregularly (not every drop splash produces bubbles) and the bubbles vary widely in size. Thus the acoustic signal from these drops is spread over a wide frequency range (1–50 kHz), which allows the large drops to be detected when they are present. In the laboratory studies, the largest drops produced the largest bubbles, and thus lowest frequency (order 1 kHz) sound, suggesting that several large drop size categories might be separable acoustically. However, only two large drop size categories appear to be separable acoustically. These are ''large'' (2.0–3.5-mm diameter) and ''very large'' (greater than 3.5-mm diameter).

The very large raindrops are extraordinarily loud underwater. They are strongly deformed by air drag and are flattened on the leading edge of the drop. This acts as a ''hammer'' on the water surface, causing the impact component of sound generated by the raindrop to be a strong function of drop diameter, at least the 6th power (Medwin et al. 1992). The signal from this impact is a broadband sound (white noise) extending from at least 1–50 kHz. Very large raindrops also produce penetrating turbulence (Green and Houk 1979), which allows the entrained bubbles to be mixed downward. This ''mixing'' by very large raindrops affects the shape of the underwater sound spectrum by generating an absorbing layer of small bubbles near the water surface.

Table 2 summarizes the physics of the drop splash associated with each drop size.

4. The acoustic inversion

a. Building the acoustic inversion

A sound source at a free surface, the ocean surface, is an acoustic dipole, radiating sound energy downward

in a $\cos^2\theta$ pattern where θ is the zenith angle. This allows the intensity of sound at some depth h below the surface to be given by

$$I(h) = \int I_0 \cos^2\theta \text{atten}(p)\, dA, \tag{7}$$

where I_0 is the sound intensity at the surface and atten(p) describes the attenuation due to geometric spreading and absorption along the acoustic path p. Absorption of sound in the ocean is frequency dependent, depending on the nature of the water (salinity, pressure, chemical composition) and the bubble density along the path. Because the speed of sound varies, acoustic refraction occurs; however, for short distances, this is a minor correction and spherical spreading p^{-2} is a good approximation. Furthermore, because most of the energy is arriving at steep angles, even in strongly refracting environments this is only a minor correction—typically less than 1 dB (see, e.g., Vagle et al. 1990). If the acoustic paths are assumed to be straight, then Eq. (7) can be written as

$$I(h) = \int I_0 \cos^2\theta \frac{\exp(-\alpha p)}{4\pi p^2}\, dA, \tag{8}$$

where α is the absorption coefficient. In the ocean, the absorption coefficient is a strong function of frequency ranging from 0.5 dB km^{-1} at 1 kHz to 10 dB km^{-1} at 40 kHz (Medwin and Clay 1998). It is much less in freshwater. Equation (8) can be used to estimate an effective listening area. For example, if the sound source is assumed to be uniform on the ocean surface and absorption is neglected, then 50% of the sound energy arrives from an area equal to πh^2 over the hydrophone and 90% of the sound energy arrives from an area equal to $\pi(3h)^2$, where h is the depth of the measurement hydrophone. The integrating area of the hydrophone is important for a couple of reasons. First, rainfall is inhomogeneous on all scales, but rainfall measurements are needed on large temporal or spatial scales. An instrument with a large inherent sampling area should produce a better ''mean'' rainfall statistic. Second, because the sound sources are discrete events, individual splashes, and the spectrum of any single raindrop is variable in spectral character (except for small raindrops), it is important to integrate over many events to produce a ''smooth'' mean spectrum. It is the ''mean'' spectrum of the individual raindrop sizes that is used to decompose the observed sound.

Equation shows that the observed sound intensity at the hydrophone is associated with the sound intensity at the surface, modified by attenuation. The sound intensity, I_0, at the surface is related to the drop size distribution in the rain by

$$I_0(f) = \int A(D, f) V_T(D) N(D)\, dD, \tag{9}$$

where f is frequency, $A(D, f)$ is the transfer function describing the radiated sound as a function of frequency for a given drop size D, V_T is the terminal velocity of the drop, and $N(D)$ is the drop size distribution in the rain. In a measurement situation, this equation is discrete and given by

$$\mathbf{I}_0(f) = \mathbf{A}(D, f) \cdot \mathbf{DRD}(D), \tag{10}$$

where **DRD** is the drop rate density, $\mathbf{DRD} = V_T \cdot N(D)$. If the inversion matrix **A** is known, then, using singular value decomposition, Eq. (10) can be inverted:

$$\mathbf{A} = \mathbf{U}\Lambda\mathbf{V}^{\mathrm{T}}, \tag{11}$$

$$\mathbf{DRD} = \mathbf{V}[\Lambda^{-1}(\mathbf{U}^{\mathrm{T}}\mathbf{I}_0)], \tag{12}$$

to make a measurement of the drop size distribution in the rain.

Using the laboratory results as a guide, the field data can be decomposed to obtain mean spectral signatures for each drop size. The data were searched to find periods when the rain contained isolated populations of various drop sizes. On several occasions the rain consisted of only drops smaller than 0.8-mm diameter. The sound of drizzle, the 13–25-kHz peak, is only detected when raindrops greater than 0.8-mm diameter are present in the rain. This sets the lower size limit for small raindrops. Drops smaller than 0.8 mm are hereby called ''tiny'' and do not produce a detectable sound signal. They cannot be measured acoustically. The upper size limit for small raindrops is set to 1.2 mm based on the laboratory studies (Pumphrey et al. 1989; Medwin et al. 1992). The mean spectral signal for a small raindrop was determined by isolating rainfall conditions when only small and tiny raindrops were present, as indicated by the JW disdrometer, and then dividing the observed sound intensity by the number of small raindrops present to obtain a spectral density per drop. This signal is shown in Fig. 4.

Medium drop splashes do not generate bubbles and are therefore relatively quiet. Since the laboratory studies show that larger drops produce larger bubbles that resonate at frequencies below 10 kHz, the field data was examined to determine when sound was detected below 10 kHz, for example, see Fig. 2. Whenever the rain contains drops larger than 2.0 mm, the sound levels below 10 kHz were high. Thus, the lower size limit for large raindrops was set at 2.0 mm. This defines the medium drop size to be 1.2–2.0-mm diameter. To obtain a spectral signature for these drops, times when the rain contained only tiny, small, and medium drops were isolated. Using the spectral signature of the small drops to estimate the sound intensity due to the small drops, the remaining energy was assumed to be due to medium drops. A mean spectral density for medium drops is shown in Fig. 4. Because the small drops are so much louder than the medium drops from 13 to 30 kHz, the sound signature for the medium drops is interpolated through this frequency region. And, although the signal

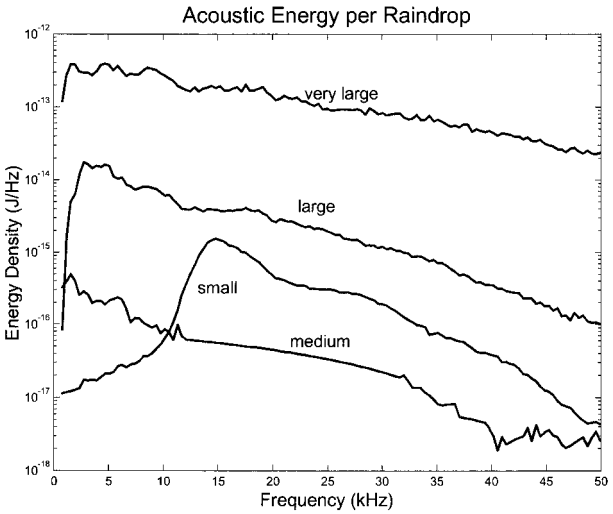

FIG. 4. The acoustic signature of individual drop size categories. This forms the basis for the inversion of the sound field to obtain drop size distribution.

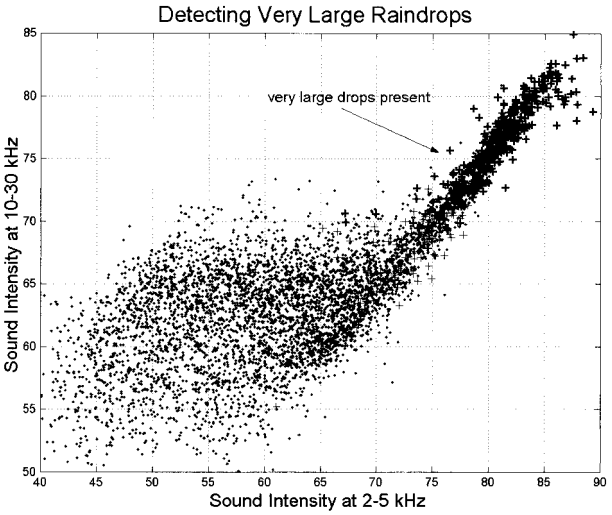

FIG. 5. A comparison of sound intensity at 2–5 and 10–30 kHz. The detection of very large raindrops in the rain can be achieved using these two frequency bands.

from the medium drops is small, it is louder than expected from the laboratory studies. Presumably, this sound is from the impact of the drop onto the water surface and should be a broadband signal as shown.

Large drops are loud underwater. But the sound generated by any individual large drop is at the very narrow bands associated with any bubbles that are generated plus a broadband signal from the impact. When averaged over many individual drop splashes, the mean spectrum for a large drops size becomes smooth (Fig. 4). The laboratory results (Medwin et al. 1992) show that larger drops produce, on average, larger bubbles. The largest bubbles also tended to be loudest, producing a spectral peak in the mean spectrum at the resonance frequency of these ''dominant'' bubble sizes. This suggests that several large drop size categories can be identified acoustically. Attempts to ''fine-tune'' the spectral signatures of the large drops into, for example, four size categories, failed. Only two are shown in Fig. 4. But, the result is consistent with the laboratory findings. The spectral peak for the ''large'' drops is between 2 and 5 kHz, while the very large drop category shows the peak extending down to 1–2 kHz. The 2–5-kHz peak feature was often observed in the field data (Fig. 1).

The drop size boundary between the large (2.0–3.5-mm diameter) and very large (>3.5-mm diameter) drop size categories is illustrated in Fig. 5. Whenever very large raindrops are present in the rain, the sound level increases sharply at all frequencies. This is consistent with recordings of underwater sound during rain containing very large raindrops, during which loud ''smacks'' from drop impacts are clearly heard. Isolated periods of data when only very large drops were present were used to identify the mean spectrum for very large drops (Fig. 4).

In summary, Eq. (12) is the formulation for the inversion of the sound field and Fig. 4 is a graphical representation of the transfer function $A(D, f)$. Given a sound spectrum, a drop size distribution will be mathematically calculated, however it may be unrealistic. Thus, a constrained inversion is proposed.

The mathematical inversion allowed partial values of very large raindrops to be present. Of course, these drops are either present or they are not present. If partial values of very large drops are predicted, the inversion compensates by underestimating the smaller drop size category populations. Since the sound energy radiated by very large raindrops is relatively large compared to their water volume, this compensation results in an underestimation of rainfall rate. To address this problem, the inversion is attempted and if the number of very large drops is greater than a chosen value, 10 m^{-2} s^{-1}, then very large drops are assumed to be present. If they are not present, the inversion is repeated with the very large drop population forced to be zero.

A second problem is that the medium raindrops have a weak acoustic signal. They are hard to hear, especially if very large raindrops are present. In fact, unrealistic values of the medium drop category are common. Unfortunately, medium-sized raindrops often comprise a significant part of the liquid content of rainfall, and so accurate estimates of their populations are important. To address this problem, if very large raindrops are detected within the rain, it is assumed that the medium drops that might be present cannot be heard. No attempt is made to acoustically invert for the medium drop population. Instead, the medium drop population is set based on the small drop population count. On the other hand, if very large raindrops are not detected, then an acoustic inversion estimate of the medium drop population is obtained from the singular value decomposition with the very large drop population set to zero. Fur-

thermore, the resulting drop size distribution is constrained to be monotonically decreasing with drop size above the medium drop size category. Finally, the medium drop count is not allowed to be greater than twice the small drop population. These last two constraints are artificial, but are consistent with most of the observed drop size distributions recorded by the JW disdrometer.

b. Algorithm performance

Figure 6 shows some examples of the performance of the inversion for several of the cases in Table 1. Both the inversion, estimating the drop size distribution given the sound field, and the forward problem, estimating the sound field given the drop size distribution are shown. In general, the predictions match the observations, although there is one situation where consistent disagreements are present.

During extremely heavy rainfall, the forward problem overestimates the observed sound levels above 10 kHz, often by many decibels (Fig. 6a). In fact, the sound levels above 30 kHz can often become less than those observed at lighter, but still very high, rainfall rates (cf. Figs. 6a and 6b). Since heavier rain has more sound sources present, the best explanation for this observation is attenuation by small bubbles below the water surface. These bubbles are presumably mixed downward by the turbulence of the very large raindrop splashes, forming a layer through which newly generated sound (at the surface) must pass. The smallest bubbles will remain in the water longest, due to buoyancy, and thus the attenuation is greatest at the higher frequencies. Since attenuation by air bubbles is strongly dependent on bubble size [Eq. (5) or Medwin and Clay 1998, chapter 8], the size of bubbles present in this layer can be identified. For this example, the bubbles range in size from about 200-μm radius (resonance at 15 kHz) down to less than 60-μm radius (resonance at 50 kHz).

The overall performance of the inversion for each drop size category is shown in Fig. 7. Only four drop size populations are measured. No attempt is made to estimate the tiny drop population count. These drops are silent and the JW disdrometer data showed that this population count was unpredictable, often higher or lower than the small drop population density. The medium and large drop categories often contain a large percentage of the total water content of the rain, and so accurate estimates of their populations is important. Figure 7 shows that both of these drop size categories are fairly well estimated. Based on the correlation coefficient between disdrometer and acoustic drop counts, the very large drop category is the most difficult to estimate accurately. However, the numerical count for the very large drops is relatively low compared to the smaller drop categories and so errors in the populations of very large drops do not lead to large errors in total rainfall rate. More important is to simply detect whether or not the very large raindrops are present in the rain (Fig. 5) and then to use this information to constrain the inversion. Table 3 summarizes the success of the very large drop detection. Very large (vl) raindrops were present and detected 7.8% of the time (correct decision). False detection (vl drops detected acoustically, but not present) occurred 2.3% of the time, and undetected drops (vl drops not detected acoustically, but present) occurred 2.4% of the time. Of course, most of the time vl drops are not present and not detected by either instrument (87.5% of the time).

Once drop size distribution has been determined, a variety of rainfall measures can be calculated. When calculating rainfall rate, the representative drop size for the four acoustic drop size categories (small, medium, large, and very large) are 0.98, 1.6, 2.5, and 3.7 mm, respectively. These values were calculated by using the higher resolution JW disdrometer data to find the equivalent drop size within each drop size category, which produced the observed rainfall rate from the measured drop size distribution (the JW disdrometer data) over each drop size range. These equivalent drop sizes change depending on the moment of the drop size distribution desired. An alternative approach is to fit an analytic expression [Eq. (1) or (2)] to the discrete acoustic inversion values and then to integrate using the analytic distribution.

The performance of the inversion to obtain rainfall rate is shown in Fig. 8. For these data, the acoustic accumulation total is 900 mm, compared to 969 mm from the disdrometer, 963 mm from the capacitance rain gauge, and 1031 mm from the optical rain gauge. For more on the intercomparison of these gauges, see Nystuen (1999). The overall correlation between the logarithms of the disdrometer rainfall rate and the acoustic inversion rainfall rate is 0.90; however, there are some outliers. These outliers were examined individually to determine if there were systematic errors associated with particular environmental conditions or rainfall drop distributions (Fig. 9). A few of the outliers are associated with timing offsets between the disdrometer and acoustic data, and will not be considered further.

Occasionally ''irregular'' drop size distributions are present. An example is shown within the transition phase of the mesoscale convective system event in Fig. 10. At min 310, the disdrometer data shows a bimodal distribution in the drop spectrum, where a large drop peak gradually shifts to smaller and smaller drop size. This ''size-sorting'' can occur when a collection of drops aloft fall with different velocities to the surface. The largest drops, with higher fall velocities, arrive at the surface first, and gradually the size of the drops shifts to smaller sizes as the smaller drops reach the surface later. Underwater this situation is apparently relatively loud, and the acoustic estimate of the smaller drops population, especially the medium drops, is high, causing the acoustic rainfall rate to be high relative to the disdrometer. This tendency for the acoustic rainfall rate

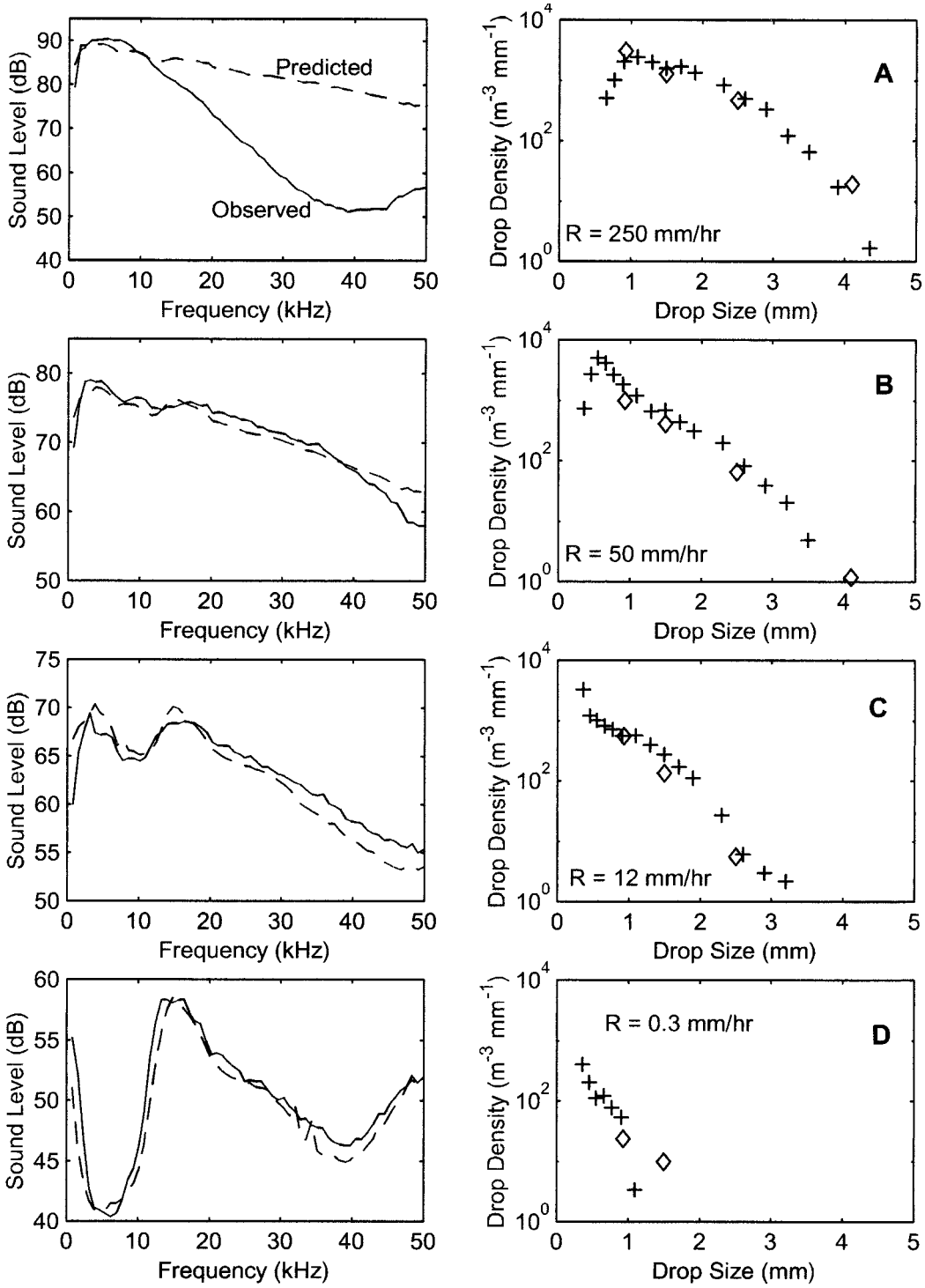

FIG. 6. Four examples of individual inversions to obtain drop size distribution. (right) The disdrometer data are shown, ''+,'' with the acoustic inversion results '' ◊.'' (left) The observed sound field (solid line) is compared to the sound field predicted from the disdrometer data using the transfer function shown in Fig. 4 (the ''forward problem''). Details for these four datasets (IDs = 114_33, 256_39, 256_50, and 256_68, respectively) are given in Table 1.

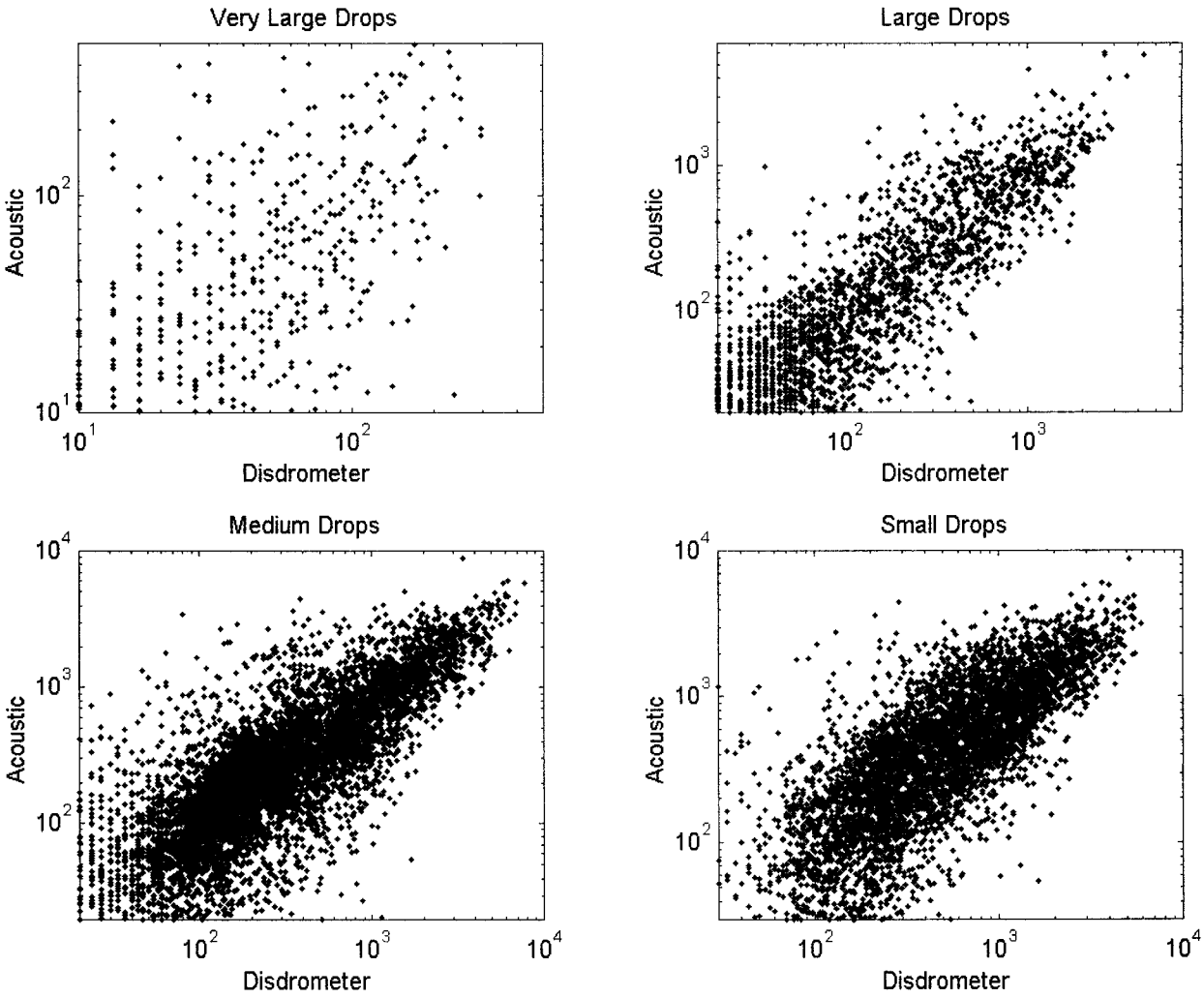

FIG. 7. The acoustic inversion drop count for each drop size category compared to the JW disdrometer drop count for the same drop size range. Data are from over 6000 min of rainfall from Apr to Dec 1994. The units are counts m^{-2} s^{-1}. The correlation coefficients for the logarithm of the counts are $r = 0.56$ (very large drops), $r = 0.86$ (large drops), $r = 0.77$ (medium drops), and $r = 0.76$ (small drops).

to be high relative to the disdrometer was also present during stratiform II rain when there are relatively more large raindrops present. And on a few occasions at the start of convective events (ic), the rain consisted of very large raindrops and relatively few smaller drops causing the acoustic rainfall rate to be very high relative to the disdrometer (Table 1, example ic161_6).

There are also examples of the opposite problem—undetected medium drops. Occasionally, the drop size distribution has relative maximum in the medium drop size category. These drops are relatively quiet underwater, and generally the situations with relatively more medium drops are missed acoustically, causing an underestimation of rainfall rate relative to the disdrometer.

A final environmental factor considered was wind speed. In fact, the experimental location was partially

TABLE 3. Choice of inversions. Three acoustic inversions were used: very large (vl) raindrops present; large (lg), medium, and small drops present; and only medium and small (me/sm) drops present. The data considered here are 5315 min of rainfall between Apr 1994 and Dec 1994 when the rainfall rate exceeded 0.1 mm h^{-1}.

		Disdrometer detection		
		vl present	lg present	me/sm only
Acoustic Dectection	vl present:	416 (7.8%)	121 (2.3%)	0
	lg present:	130 (2.4%)	2407 (45.3%)	295 (5.5%)
	me/sm only:	0	412 (7.8%)	1534 (28.9%)

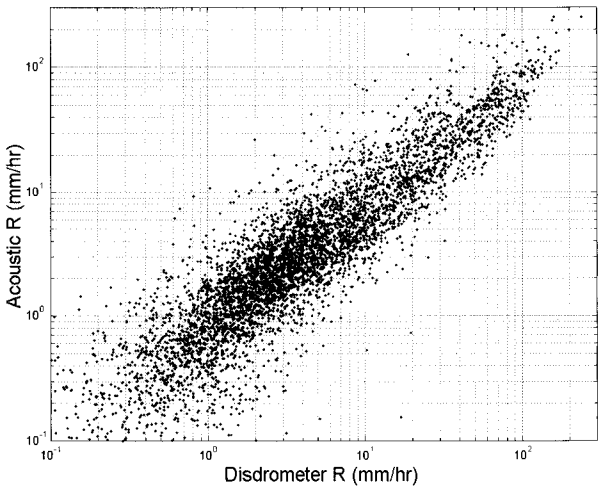

FIG. 8. Acoustic rainfall rate compared to disdrometer rainfall rate for over 6000 min of rainfall from Apr to Dec 1994. The correlation coefficient between the logarithms of the rainfall rate is $r = 0.90$.

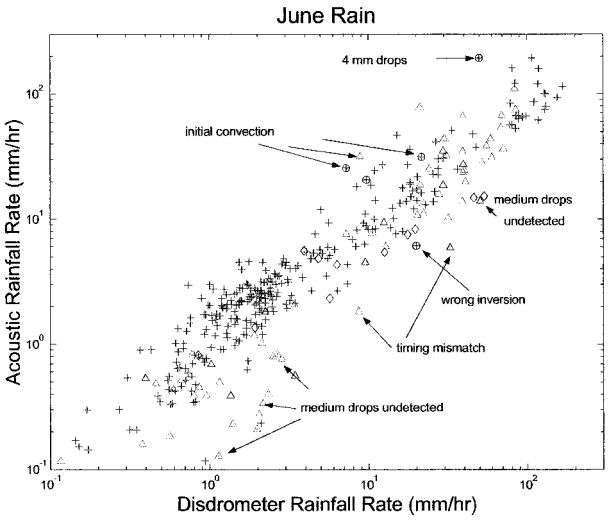

FIG. 9. A detailed examination of Jun 1994 rainfall to determine the cause of outliers. The different symbols correspond to different individual events during the month.

sheltered from wind by the mangrove trees surrounding the pond. Much of the time the local wind was less than 2 m s^{-1}, but there were a few events where the wind speed was over 5 m s^{-1}. This range of wind speeds is small, but was sufficient to show the effect of wind on the acoustical small drop counts (Fig. 11). When compared to the calm (<2 m s^{-1}) situation, the acoustic small drop count is three times lower under windy conditions (>5 m s^{-1}). This is expected from the laboratory studies (Medwin et al. 1990) and field studies (Nystuen 1993), which show that the sound production mechanism for small raindrops is sensitive to angle of impact. There was no apparent influence of wind on the drop population counts of the larger drop size categories.

An alternate acoustic estimate of rainfall rate is to develop an empirical relationship between the sound level within a particular frequency band and rainfall rate, as measured by one of the other rain gauges (Nystuen et al. 1993). This is demonstrated for two different frequency bands, 2–5 and 4–10 kHz, in Fig. 12. The proposed relationships are

$$\log_{10} R = (\mathrm{SPL}_{25} - 51.5)/17 \quad \text{and} \tag{13}$$

$$\log_{10} R = (\mathrm{SPL}_{410} - 50)/17, \tag{14}$$

respectively, where SPL_x is sound level in the frequency bands 2–5 and 4–10 kHz in decibels relative to 1 μPa^2 Hz^{-1}. These relationships are tuned to match the total rainfall accumulation from the disdrometer and are shown in Figs. 12a and 12b, respectively. While these relationships are easy to apply, they also contain outliers. A similar type of relationship from Nystuen et al. (1993) overestimates rainfall when the rain contains relatively more large drops. No attempt to estimate rainfall using the 10–30-kHz frequency band should be made. This is the frequency band where small raindrops produce sound. The signal from these drops is sensitive to wind speed.

Table 4 contrasts the various methods of rainfall rate estimation from the rain gauges and the acoustic methods. It shows that the acoustic inversion is an improvement over the direct acoustic methods [Eqs. (13) and (14)] just described. It has the additional advantage of being used to calculate other rainfall parameters, for examples, D_0, N_0, Z . . . .

5. Application of acoustical rainfall analysis to rainfall research issues

a. The Z–R relationship

The relationship between rainfall rate R and equivalent reflectivity Z is important to radar meteorologists as Z is the quantity sensed by radars, while R is the quantity desired by many users. To better understand the Z–R relationship, it has been partitioned in a variety of ways (e.g., Ulbrich and Atlas 1978, 1998; Tokay and Short 1996; Atlas et al. 1999). The Z–R diagram for the Miami rainfall dataset, calculated using the JW disdrometer data, is shown in Fig. 13. Theoretically, artificial drop size distributions can be designed to occupy any part of the Z–R diagram. In Fig. 13 the Miami data have been partitioned based on the acoustic detection of specific drop size populations. In particular, one partition is for rainfall containing very large (over 3.5-mm diameter) drops. Another partition is for rainfall containing large raindrops, but no very large drops. And the third partition is for rainfall containing no large or very large drops (no drops >2.0-mm diameter). Table 3 shows the overall distribution of these three acoustic rainfall classifications. These acoustic partitions demonstrate that for naturally occurring rain (the Miami

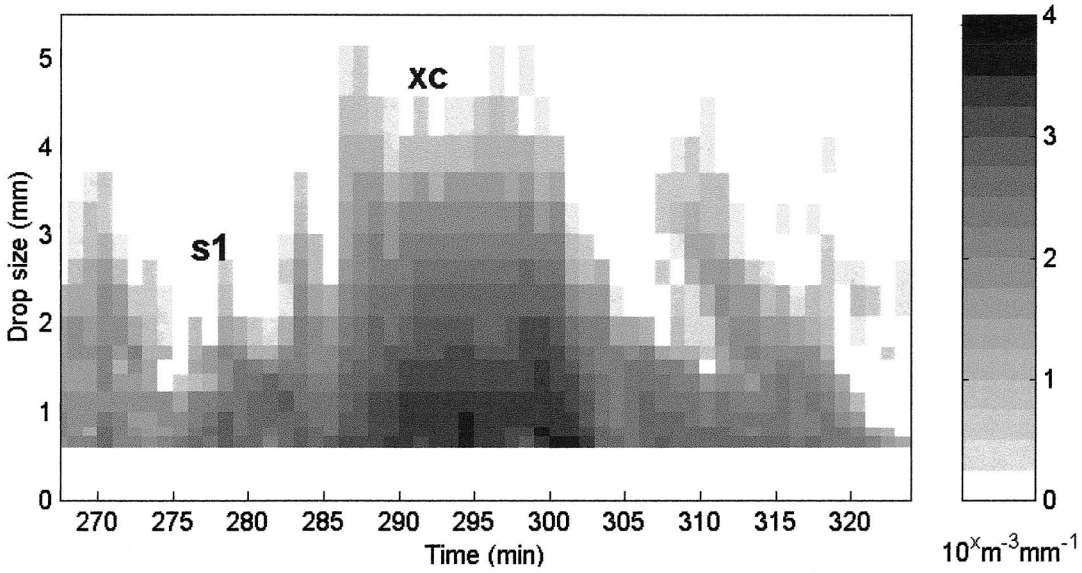

FIG. 10. An example of an unusual drop size distribution. The disdrometer shows a bimodal drop size distribution with relatively few medium-sized drops at min 310. The acoustic inversion overestimates the medium drop population leading to an overestimation in rainfall rate.

data), different parts of the *Z–R* relationship are associated with the presence or absence of specific drop size populations within the rain.

The acoustic partition shown in Fig. 13 uses the acoustic inversion choice (Table 3). Nearly equivalent partitioning is available using the sound level at 2–5 kHz (Fig. 5). If $SPL_{25} > 73$ dB then very large raindrops are present in the rain. If $SPL_{25} < 60$ dB, no large or very large drops are present.

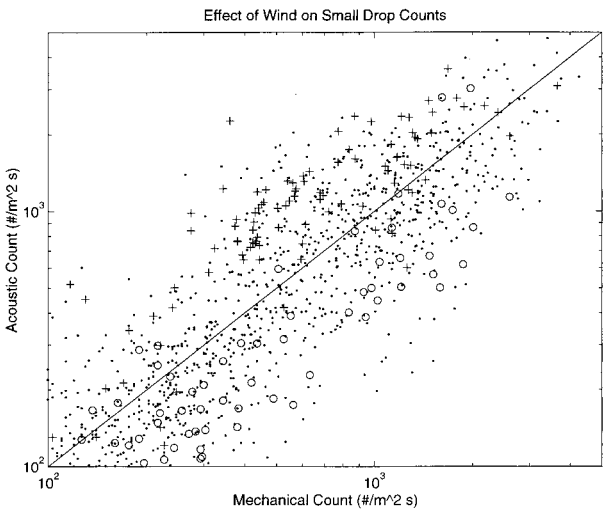

FIG. 11. The effect of wind on the small drop population count during TS Gordon (Nov 1994). During windy conditions ($U > 5$ m s^{-1}, "○" symbol) the acoustic small drop count is a factor of 3 lower than during calm conditions ($U < 2$ m s^{-1}, "+" symbol). Intermediate wind speed (2 m $s^{-1} < U < 5$ m s^{-1}) points are shown by the "●" symbol.

b. Classification of rainfall

It is generally felt that at least two measures of the rainfall drop size distribution are needed to effectively describe the rain (Ulbrich and Atlas 1978). As the acoustical inversion of the underwater sound is sensitive to at least two different raindrop populations within the rain, there is promise that the acoustical technique can be used to classify rainfall types (Black et al. 1997). This ability to classify rainfall type ultimately depends on the requirement that different types of rainfall have unique drop size distributions at the ocean surface where the sound is generated.

Examination of the sound spectra during rainfall (Fig. 1 or 2) suggests that at least four classifications of rainfall are likely using underwater sound. For most applications the goal is to identify stratiform, a light widespread type of rain, and convective, a heavier rainfall with shorter space and timescales. From Fig. 2, it appears that there are two types of stratiform rain, and that these are distinguishable acoustically. These two rainfall types are identified in Atlas et al. (1999) as types I and II. In their study, type II stratiform rainfall is associated with a strong brightband aloft, a feature that cannot be "heard" below the water surface.

To identify periods of stratiform and convective rainfall, Black et al. (1997) proposed a discriminant based on the shape of the acoustic spectrum. Their exact expression included the background noise levels associated with specific sites and events that are inappropriate and unnecessary for universal application. During rainfall, the sound levels are almost always well above the local noise. If not, then rainfall should not be measured acoustically. However the revised discriminant defined

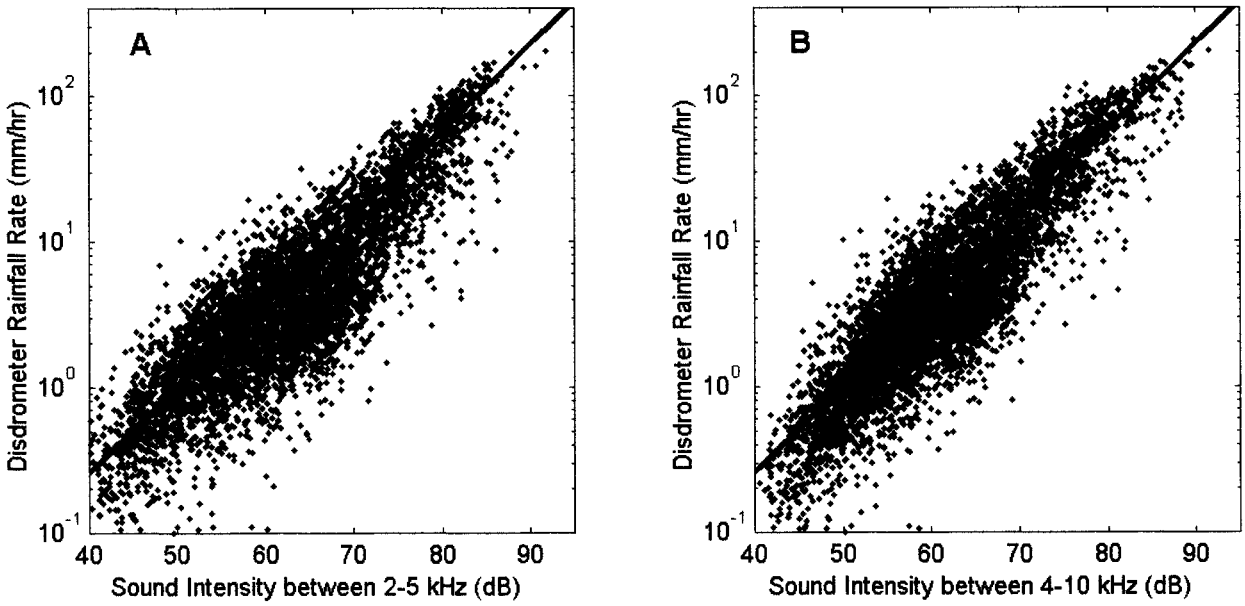

FIG. 12. The comparison of sound pressure levels and disdrometer derived rainfall rates for the frequency band 2–5 kHz (Fig. 12a) and 4–10 kHz (Fig. 12b). Equations (13) and (14) are shown for each dataset, respectively.

by Eq. (4), the ratio of the sound level between 10 and 30 kHz divided by the sound level between 4 and 10 kHz, is essentially identical to the Black et al. discriminant. It has a positive value in situations when the rain contains no large raindrops as Black et al. suggest. This includes most of the stratiform I rainfall category (see Table 1). However, its value depends on the relative proportions of large raindrops, which produce sound from 4 to 10 kHz, and small drops, which produce sound from 10 to 30 kHz. Unfortunately, within the stratiform II rainfall conditions, there are large drops present and relatively fewer small drops. In these conditions, this drizzle discriminant fails to classify the rainfall as stratiform (Fig. 3e or Table 1). On the other hand, acoustic classification is clearly possible using two measures of the sound field (Fig. 14). Figure 14 shows that the different rainfall types do have distinguishable characteristics, but that the ratio between the sound level at 10–30 kHz and 4–10 kHz is not sufficient to distinguish between extreme convection and stratiform II type rainfall.

TABLE 4. A comparison of rainfall rate measurements for 5174 min of rainfall greater than 0.1 mm h^{-1} between Apr 1994–Dec 1994. The correlation coefficients are for $\log_{10}R$, where the rainfall rate R is from the disdrometer R_d, the optical rain gauge R_o, the capacitance rain gauge R_c, the acoustic inverse R_{inv}, and the sound levels at 2–5 and 4–10 kHz, R_{25}, and R_{410}.

	R_d	R_c	R_o	R_{inv}	R_{25}
R_c	0.89				
R_o	0.94	0.91			
R_{inv}	0.90	0.85	0.87		
R_{25}	0.86	0.81	0.79	0.90	
R_{410}	0.88	0.83	0.82	0.93	0.98

A second acoustic discriminant [Eq. (5)] may also prove to be useful. This discriminant is the ratio between the sound level at 4–10 kHz (sensitive to large drops) and the sound level between 40 and 50 kHz. This attempts to detect the distortion of the sound spectrum by subsurface bubbles (Fig. 6a) that is observed during extremely heavy convection, with $R > 100$ mm h^{-1}. The extreme rainfall class is easily detected because of the extremely high sound levels, and so this discriminant may not be necessary for classification of this rainfall type. But identification of bubble injection into the ocean is an indicator of potential gas exchange and of strong vertical stirring just below the ocean surface. From these data, if this discriminant is greater than 15 dB ($\text{DR}_{\text{bubbles}} > 15$ dB), then a bubble layer is likely to be present in the surface water. This discriminant should not be applied during stratiform I type rainfall, as there is no acoustic signal from this type of rain at 4–10 or 40–50 kHz (Figs. 1 or 2), and therefore one would be listening to the background ''noise'' rather than sound associated with rain. This discriminant is shown together with the drizzle discriminant in Fig. 3e.

Prior attempts to classify rainfall at the surface have relied on identification of the rainfall parameters using disdrometer data (Atlas et al. 1999). Given a drop size distribution measurement, any moment of the drop size distribution can be calculated:

$$M_x = \int D^x N(D)\, dD, \tag{15}$$

where x is the moment. Given the moments, the analytical drop size distributions [Eqs. (1) and (2)] can be fit to any set of data (Willis 1984; Ulbrich 1983, re-

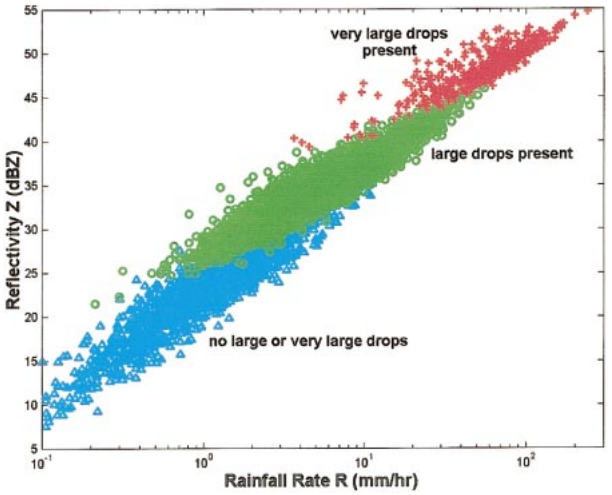

FIG. 13. The *Z–R* relationship calculated from the JW disdrometer data and partitioned by acoustic inversion choice (Table 3). Each acoustic partition is associated with the presence or absence of particular drop sizes within the rain. Very large drops are present "+"; large drops are present, but no very large drops "○"; no large or very large drops "△."

spectively). Thus, in addition to the "straight" measures of the sound field, the acoustic inversion of the sound field can be used to generate the same parameters of the drop size distribution that are calculated by drop size distributions measured by other types of disdrometers. Figures 3a–d show comparisons of the JW disdrometer measured values of R, Z, D_0, and N_0 and the acoustic values. Generally, agreement is good. Based on examination of 10–15 of the larger rainfall events containing multiple rainfall types, two of the most promising parameters to classify rainfall are N_0 and D_0. The parameter N_0 is likely to be the best measure to use to distinguish between the moderate convection and stratiform II rainfall types.

There is a tendency for the acoustic measure of N_0 to be low relative to the mechanical measure of N_0 (JW disdrometer) during extreme rainfall conditions (Fig. 3c). This appears to be associated with fitting an analytic drop size distribution [Eq. (1) or (2)] to a dataset with a limited number of drop size categories. The acoustic drop size distribution only has four drop size categories, and only two large drop size categories. In contrast, the JW disdrometer has 20 drop size categories. The shape of the large drop size distribution during extreme rainfall often showed a curvature that cannot be expressed using a limited number of drop bins. This curvature is well modeled by the shape parameter μ from the gamma distribution [Eq. (2)]. Figure 15 shows a comparison of the gamma distribution parameters from the JW disdrometer and the acoustic inversion for the same rain event shown in Fig. 3. During the extreme rainfall conditions, μ is much higher for the JW distrometer. Surprisingly, this does not affect the measurements of the other rainfall parameters (R, Z, D_0, etc.). Figure 16 shows a detailed single inversion with the gamma distribution fit shown for both the JW disdrometer and the acoustic inversion. In both cases, the rainfall rate calculated from the data points or the analytical fits (the gamma distribution curves) match. The difference is the fit to the curvature of the large drop size densities. [Note that the gamma distribution does not always "fit" the small drop size densities very well. It is more sensitive to the larger drop sizes (Ulbrich and Atlas 1998).] The μ parameter is a "shape" parameter and is not necessarily associated with the rainfall type. Indeed, examination of the μ values for the different rainfall types considering only values from the JW disdrometer show that there is no consistent pattern or value (Table 1).

c. *Temporal analysis of rainfall*

One obvious application of the acoustic analysis of rainfall is the very high temporal resolution that is possible. The sampling area for the acoustics is a function of hydrophone depth and can be orders of magnitude greater than the other in situ rain gauges (disdrometer, optical rain gauge, etc.). This implies that a large sample size of the rain can be obtained in a much shorter period of time. Indeed, throughout this paper, the sound field has been averaged to one minute resolution to allow intercomparison with the other rain gauges. However, the acoustic spectra show temporal variability on a much shorter timescale, especially during convective rainfall. The temporal details of the extreme convection for event 150 at 0113 (Figs. 2, 3, 14, and 15) using the acoustic inversion with 5-s resolution are shown in Fig. 17. For comparison, 1-min rainfall rate data from the disdrometer and the capacitance rain gauge are shown. None of the other rain gauges can show the intraminute variability of the rain, nor do they show the rapid onset or cessation of the subcells within the rain. These subcells have timescales of 2–5 min within this example, but are poorly defined and appear with a time lag using the other rain gauges. As the rainfall changes from extreme convection to transition (min 150–175, see Figs. 2 or 3), and then to stratiform (after min 175), the short timescale variability within the rain is much diminished.

6. Conclusions

An inversion of the underwater sound field to obtain quantitative measurements of the drop size distribution in rain has been described. This inversion algorithm is based on knowledge of the physics of underwater sound production by four acoustically distinctive drop size categories, each of which has different splash physics (Table 2). Distinctive acoustic signatures for these drop sizes (Fig. 4) are obtained from the selective decomposition of field data and form the basis for a constrained mathematical inversion of measured sound fields. This inversion algorithm has been applied to thousands of minutes of acoustic rainfall data and compared to other

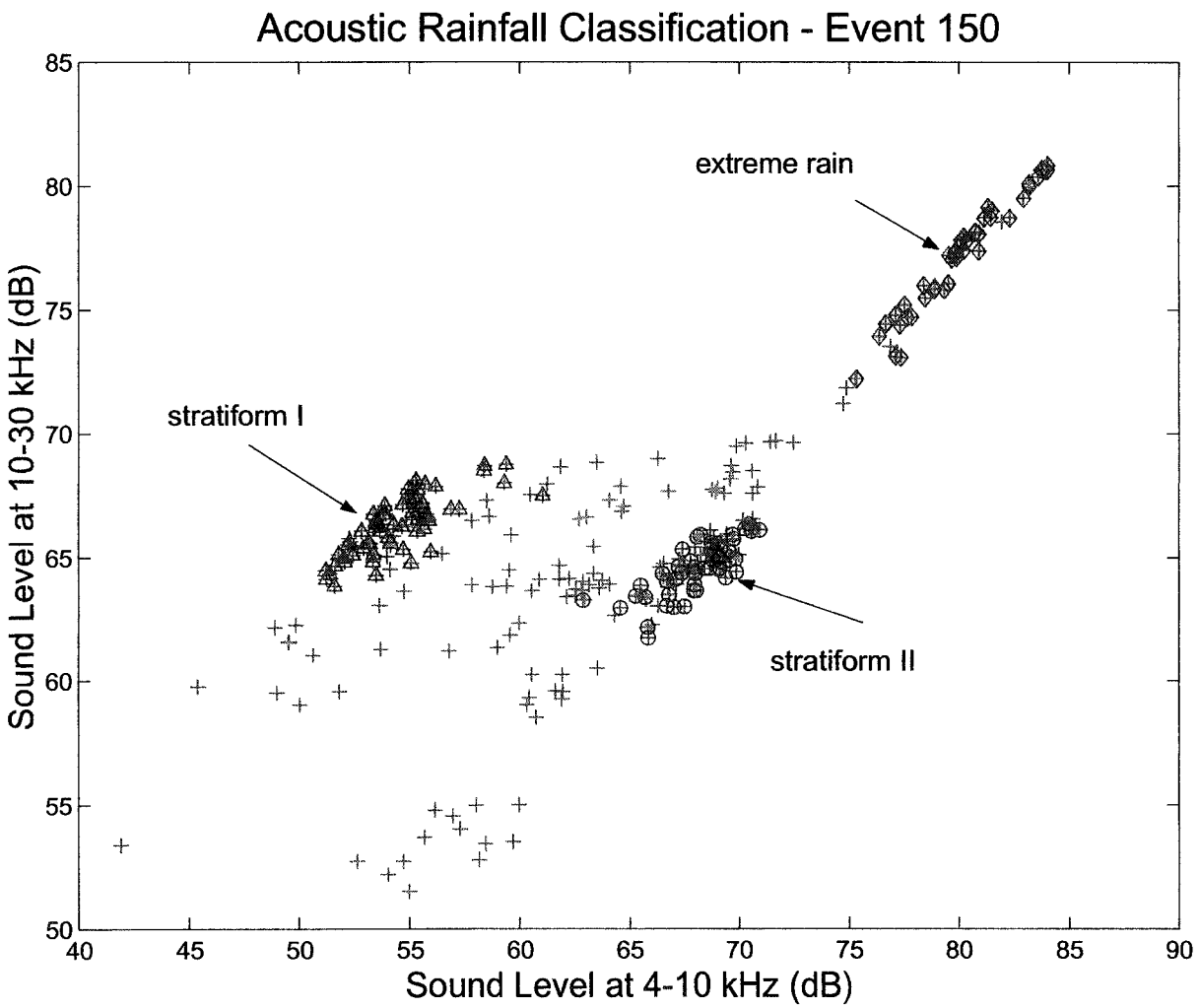

FIG. 14. The acoustic classification for event 150 at 0113. The data points for different rainfall types (extreme convection, stratiform I and II) are separated using a comparison of the sound levels at a lower frequency (4–10 kHz) and a higher frequency (10–30 kHz). This event is also shown in Figs. 2 and 3.

rain gauges (Nystuen 1999) including a JW disdrometer. The overall performance of the acoustic inversion to measure rainfall rate, when compared to the other rain gauges, has a correlation coefficient of about $r = 0.9$. This is slightly higher than that of simpler acoustic regression algorithms using a single frequency [Eqs. (14) or (15)]. Furthermore, by measuring drop size distribution, other integrated measures of the rainfall can be calculated.

By comparing the acoustically obtained drop size distributions to the JW disdrometer data, two problems associated with the acoustic inversion are identified. Very large raindrops (diameter >3.5 mm) are extraordinarily loud underwater. When present these drops make acoustic detection of smaller drops difficult, leading to potential errors in the estimation of the smaller drop size populations, especially the medium drops (1.2–2.0-mm diameter) category. Fortunately the very large drops can be detected acoustically, allowing a conditional inversion based on their absence or presence. These drops are dynamically important as their presence is associated with convective rain and their splashes are capable of mixing bubbles down into the upper surface layer of the water, potentially affecting gas exchange and turbulent mixing of the water.

One category of drop sizes that is difficult to count acoustically is the medium drop category. These drops (1.2–2.0 mm) have relatively quiet splashes, as the physics of the splash does not entrain bubbles (Medwin et al. 1992). When unusual drop size distributions having relative peaks or valleys in the drop size distribution at the medium drop size range were recorded by the JW disdrometer, the acoustic inversion was often low or high, respectively.

Tiny raindrops (<0.8-mm diameter) are apparently silent underwater and cannot be counted acoustically. The inability to measure these drops does not lead to a large error in rainfall rate, or other high moments of the

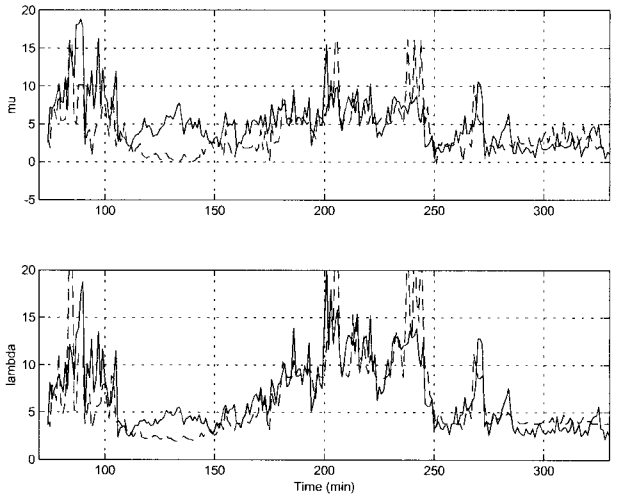

FIG. 15. The gamma distribution [Eq. (2)] shape parameters calculated by the method of moments (Ulbrich 1983) using the disdrometer data (solid line) and the acoustic inversion (dashed line) for event 150 at 0113. There is general agreement, except during the extreme convection from min 110 to 150. This event is also shown in Figs. 2, 3, and 14.

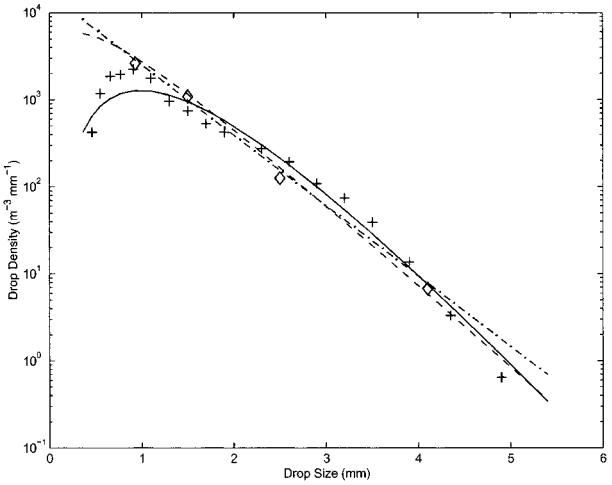

FIG. 16. An example of analytical fits [Eqs. (1) and (2)] to the JW disdrometer and acoustic inversion data for a single minute of rainfall during extreme convection (min 33 of the rainfall event on day 256; ID = 256_33—see Table 1 for details). The rainfall rate is over 100 mm h^{-1}. The JW disdrometer data (+) are fit with a gamma distribution (solid line) with $\mu = 3.0$ or an exponential distribution [Eq. (1)] (dash–dot line) ($\mu = 0$). The acoustic inversion ($\diamond$) are fit with a gamma distribution [Eq. (2)] (dashed line) with $\mu = 0.7$.

drop size distribution, for example, reflectivity, as these drops usually do not contribute significantly to the higher moments of the drop size distribution. In contrast, small raindrops (0.8–1.2 mm) are relatively loud underwater and can be measured acoustically, although the signal from these drops is affected by angle of impact (Medwin et al. 1990) and therefore by wind (Fig. 11). The Miami dataset used in this study had relatively low wind conditions and thus this issue needs to be examined in more exposed situations (Nystuen et al. 2000).

Classification of rainfall type is an important issue for meteorologists as different types of rainfall affect atmospheric heating (Houze 1989) and the performance of other rain monitoring instruments (radars, optical rain gauges) in different ways. Based on qualitative analysis of mesoscale convective systems (Atlas et al. 1999), the sound field can be used to distinguish rainfall type, at least the extreme convective, transition, and stratiform I and II categories. The discriminant proposed by Black et al. (1997) does a good job of identifying stratiform I rainfall but needs to be augmented by other acoustic sound field features such as the absolute sound level from 4 to 10 kHz in order to be able to identify stratiform II rainfall. The stratiform II rainfall is associated with a strong ''brightband'' in the Atlas et al. (1999) study.

Although only four drop size categories are measured acoustically, this is sufficient to track several of the integrated rainfall parameters that have been identified as useful for the classification of rainfall, including D_0, N_0, R, and Z. However, one set of drop size distribution shape parameters, the gamma distribution [Eq. (2)] parameters are often in disagreement with the JW distrometer derived values during extremely heavy convection. This observation indicates that the acoustic inversion cannot be used to study details of the shape of the drop size distribution, but also shows that the shape parameters are not useful indicators of rainfall type. Indeed, examination of the shape parameter μ, considering only JW distrometer data, show unpredictable values for μ across different rainfall types (Table 1).

The Z–R diagram has been examined acoustically

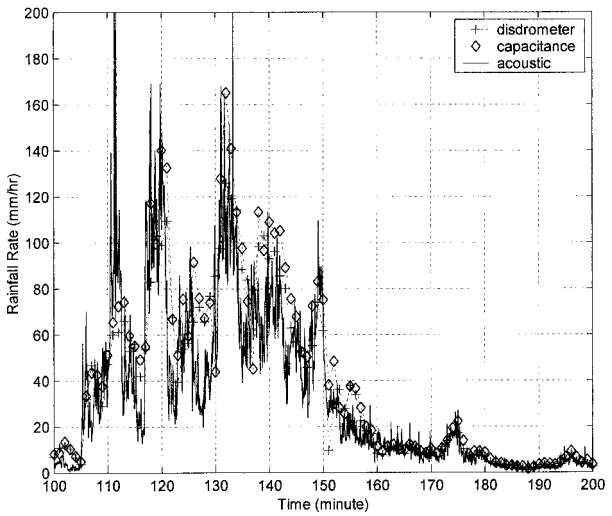

FIG. 17. High temporal resolution of the onset of the extreme convection during event 150 at 0113. The acoustic inversion has been applied with 5-s resolution (solid line) and shows rapid onset and cessation of subcells with the rain. Other rain gauge data shown with 1-min resolution are the disdrometer (+) and the capacitance gauge ($\diamond$). This event is also depicted in Figs. 2, 3, 14, and 15.

(Fig. 13) and shows that while artificial drop size distributions can be designed to occupy any part of the diagram, different parts of the diagram are, in fact, associated with the absence or presence of specific drop populations. In particular, the presence of very large raindrops (drops >3.5 mm), or the absence of any large or very large raindrops (all drops <2.0 mm) are acoustical rainfall ''classifications'' that occupy specific parts of the *Z–R* diagram.

Extremely high temporal analysis of rainfall is also possible acoustically. This analysis reveals subcells within the convective rainfall with timescales of 2–5 min showing extremely rapid onset and cessation of rain at timescales shorter than can be measured by the other rain gauges. And indeed, within these subcells there are variations on intraminute timescales. These shorter timescales are easily monitored acoustically and should be another indicator of rainfall type.

Acknowledgments. The data for this study were collected by the Ocean Acoustics Division, Atlantic Oceanographic and Meteorological Laboratory, NOAA, led by John Proni, Peter Black, and John Wilkerson. Discussions with Eyal Amitai, UMBC, and others at the TRMM workshop in Salt Lake City, Utah, on 22–24 May 2000 helped to identify scientific issues associated with rainfall drop size distributions. I wish to thank three anonymous reviewers for their thoughtful comments. Funding is from NSF Physical Oceanography, ONR Ocean Acoustics, and the NASA TRMM Office.

REFERENCES

Atlas, D., C. W. Ulbrich, F. D. Marks, E. Amitai, and C. R. Williams, 1999: Systematic variation of drop size and radar–rainfall relations. *J. Geophys. Res.*, **104,** 6155–6169.

Black, P. G., J. R. Proni, J. C. Wilkerson, and C. E. Samsury, 1997: Oceanic rainfall detection and classification in tropical and subtropical mesoscale convective systems using underwater acoustic methods. *Mon. Wea. Rev.,* **125,** 2014–2024.

Green, T., and D. F. Houk, 1979: The mixing of rain with near-surface water. *J. Fluid Mech.,* **90,** 567–588.

Houze, R. A., Jr., 1989: Observed structure of mesoscale convective systems and implications for large scale heating. *Quart. J. Roy. Meteor. Soc.,* **115,** 425–461.

Longuet-Higgins, M. S., 1990: An analytic model of sound production by raindrops. *J. Fluid Mech.,* **214,** 395–410.

Marshall, J. S., and W. M. Palmer, 1948: The distribution of raindrops with size. *J. Meteor.,* **5,** 165–166.

Medwin, H., and C. S. Clay, 1998: *Fundamentals of Acoustical Oceanography.* Academic Press, 712 pp.

——, A. Kurgan, and J. A. Nystuen, 1990: Impact and bubble sound from raindrops at normal and oblique incidence. *J. Acoust. Soc. Amer.,* **88,** 413–418.

——, J. A. Nystuen, P. W. Jacobus, L. H. Ostwald, and D. E. Synder, 1992: The anatomy of underwater rain noise. *J. Acoust. Soc. Amer.,* **92,** 1613–1623.

Nystuen, J. A., 1986: Rainfall measurements using underwater ambient noise. *J. Acoust. Soc. Amer.,* **79,** 972–982.

——, 1993: An explanation of the sound generated by light rain in the presence of wind. *Natural Physical Sources of Underwater Sound,* B. R. Kerman, Ed., Kluwer Academic Publishers, 659–668.

——, 1996: Acoustical rainfall analysis: Rainfall drop size distribution using the underwater sound field. *J. Atmos. Oceanic Technol.,* **13,** 74–84.

——, 1999: Performance of automatic rain gauges under different rainfall conditions. *J. Atmos. Oceanic Technol.,* **16,** 1025–1043.

——, and H. Medwin, 1995: Underwater sound generated by rainfall: Secondary splashes of aerosols. *J. Acoust. Soc. Amer.,* **97,** 1606–1613.

——, and H. D. Selsor, 1997: Weather classification using passive acoustic drifters. *J. Atmos. Oceanic Technol.,* **14,** 656–666.

——, C. C. McGlothin, and M. S. Cook, 1993: The underwater sound generated by heavy precipitation. *J. Acoust. Soc. Amer.,* **93,** 3169–3177.

——, J. R. Proni, P. G. Black, and J. C. Wilkerson, 1996: A comparison of automatic rain gauges. *J. Atmos. Oceanic Technol.,* **13,** 62–73.

——, M. J. McPhaden, and H. P. Freitag, 2000: Surface measurements of precipitation from an ocean mooring: The acoustic log from the South China Sea. *J. Appl. Meteor.,* **39,** 2182–2197.

Oguz, H. N., and A. Prosperetti, 1990: Bubble entrainment by the impact of drops on liquid surfaces. *J. Fluid Mech.,* **218,** 143–162.

Pumphrey, H. C., L. A. Crum, and L. Bjorno, 1989: Underwater sound produced by individual drop impacts and rainfall. *J. Acoust. Soc. Amer.,* **85,** 1518–1526.

Rosenfeld, D., E. Amitai, and D. B. Wolff, 1995a: Classification of rain regimes by the three-dimensional properties of reflectivity fields. *J. Appl. Meteor.,* **34,** 198–211.

——, ——, and ——, 1995b: Improved accuracy of radar WPMM estimated rainfall upon application of objective classification criteria. *J. Appl. Meteor.,* **34,** 212–223.

Shaw, P. T., D. R. Watts, and H. T. Rossby, 1978: On the estimation of oceanic wind speed and stress from ambient noise measurements. *Deep-Sea Res.,* **25,** 1225–1233.

Steiner, M., R. A. Houze Jr., and S. E. Yuter, 1995: Climatological characterization of three-dimensional storm structure from operational radar and rain gauge data. *J. Appl. Meteor.,* **34,** 1978–2007.

Tokay, A., and D. A. Short, 1996: Evidence from tropical raindrop spectra of the origin of rain from stratiform and convective clouds. *J. Appl. Meteor.,* **35,** 355–371.

Ulbrich, C. W., 1983: Natural variations in the analytical form of the raindrop size distribution. *J. Climate Appl. Meteor.,* **22,** 1764–1775.

——, and D. Atlas, 1978: The rain parameter diagram: Methods and applications. *J. Geophys. Res.,* **83,** 1319–1325.

——, and ——, 1998: Rainfall microphysics and radar properties: Analysis methods for drop size spectra. *J. Appl. Meteor.,* **37,** 912–923.

Vagle, S., W. G. Large, and D. M. Farmer, 1990: An evaluation of the WOTAN technique for inferring oceanic wind from underwater sound. *J. Atmos. Oceanic Technol.,* **7,** 576–595.

Williams, C. R., W. L. Ecklund, and K. S. Gage, 1995: Classification of precipitating clouds in the Tropics using 915-MHz wind profiler. *J. Atmos. Oceanic Technol.,* **12,** 996–1012.

Willis, P. T., 1984: Functional fits to some observed drop size distributions and parameterizations of rain. *J. Atmos. Sci.,* **41,** 1648–1661.